Dielectric-Band Photonic Crystal Nanobeam Lasers

Po-Tsung Lee, *Member, IEEE*, Tsan-Wen Lu, and Li-Hsun Chiu

***Abstract*—We investigate a mode gap confined dielectric band laser via a 1-D photonic crystal (PhC) nanobeam (NB) nanocavity with lattice gradually shifted PhC mirror. Owing to different modal symmetries, different zeroth-order dielectric mode properties, including quality (Q) factors, mode volumes, lasing thresholds, and slope efficiencies, in nanocavities with two different cavity sizes are investigated. In experiments, single-mode lasing from dielectric bands with low effective lasing thresholds is obtained. Rising of the high-order modes is also observed when we increase the PhC mirror periods for high Q factor of the zeroth-order dielectric mode. In addition, we observe the bonding and antibonding modes in beamwidth mismatched coupled NB nanocavities and switch the dominant lasing mode via spatially nonuniform carrier injection.**

***Index Terms*—Photonic crystal (PhC), nanobeam (NB), nanocavity, semiconductor laser.**

I. Introduction

In the past decade, 2-D photonic crystal (PhC) devices were once regarded as the best candidate to control the photons on-demand in planar photonic integrated circuits (PICs). Via various unique features of PhCs, for example, photonic bandgap, mode gap [1], and so on, researchers can locally confine the photons in the *PhC* nanocavities [1]–[5] with extremely low optical losses and ultra-small mode volumes close to one half-wavelength cubic [4] for realizing efficient nanolaser source. However, a huge amount of lattice periods is essential for these excellent properties in 2-D PhC nanocavities and leads to very large device footprint even larger than the micro-optic resonators [6] (micro-disks, -toroids, -rings, and so on) based on total internal reflection.

Fortunately, owing to the nature of nanophotonic design in recent years, researchers had found that the same proposal can also be achieved by 1-D PhCs on a ridge waveguide [7]–[10] (also known as the nanobeam (NB)], as shown in Fig. 1(a). Very recently, various 1-D PhC NB nanocavities have been investigated and applied to active and passive devices for planar PICs, for example, nanolasers, [11]–[13], optical filters [14], [15], bistable switches [16], optomechanical nanoresonators [17], optical nanotweezers [18], optical biosensors [19], [20], and so on. Unlike 2-D PhC nanocavities, devices based on 1-D PhC NB nanocavities not only greatly reduce the device footprint in one dimension, but also have good compatibility and flexibility for integrating in highly condensed PICs via optical waveguide accessories [14], [21].

In this study, we investigate a mode gap confined dielectric band laser via a 1-D PhC NB nanocavity with lattice gradually shifted PhC mirror. In Section II, we will show 1-D PhC NB nanocavity designs with two different cavity sizes and their different zeroth-order dielectric modal properties. The measured zeroth-order dielectric mode lasing properties from the real devices will be discussed in Section III. In Section IV, we will investigate the high-order modes in the nanocavities with large PhC mirror periods. In Section V, the bonding and antibonding modes in beamwidth mismatched coupled NB nanocavities are observed and used for switching the dominant lasing mode via spatially nonuniform carrier injection.

II. Mode Gap Confined Dielectric Band in 1-D PhC NB Nanocavities

The scheme of 1-D PhCs composed of air holes on a suspended InGaAsP NB is shown in Fig. 1(a). Important parameters include lattice constant a, air-hole radius r, NB width w, NB thickness $t_{\rm NB}$, and NB index $n_{\rm NB}$. For 1-D PhCs with $a = 360$ nm and $r/a = 0.35$ on an NB with $n_{\rm NB} = 3.4$, $w = 600$ nm, and $t_{\rm NB} = 220$ nm, the transverse-electric-like (TE-like) propagating band diagram obtained by the 3-D plane-wave-expansion method is shown in Fig. 1(b). The first two bands from low to high frequencies (curves with solid circles) are the dielectric and air bands. From their mode profiles in $|E|^2$ fields at $k_x = \pi/a$ shown in Fig. 1(b), the dielectric band can provide good gain enhancement for an active light emitter owing to good field overlapping with the dielectric region, while the air band is suitable for optical sensor due to significant field overlapping with the air region.

To form a high quality (Q) factor 1-D PhC NB nanocavity, mode gap effect [3] in PhCs can provide confinement with extremely low loss and has good flexibility in optical design by tuning different PhC parameters. For the dielectric band in 1-D PhCs with r/a_A (PhC_A) on NB, we can create a heterointerface via 1-D PhCs with r/a_B (PhC_B) on the same NB, where r/a_A is larger than r/a_B, to form the mode gap effect. As shown in the band diagram in Fig. 1(b), the frequency of the dielectric band in PhC_B (red curve with hollow circles) is lower than that in PhC_A (red curve with solid circles) on NBs. The frequency difference denoted by the shadow region forms the mode gap, where the dielectric band in PhC_A with frequency inside cannot propagate in PhC_B. Therefore, this heterointerface of PhC_A

Manuscript received July 12, 2012; revised October 03, 2012 and November 01, 2012; accepted November 18, 2012. Date of publication November 26, 2012; date of current version December 13, 2012. This work was supported by the Taiwan's National Science Council (NSC) under Contracts NSC-100-2221-E-009-109-MY3, NSC-101-2221-E-009-054-MY2, and NSC-101-3113-P-009-004.

P.-T. Lee and T.-W. Lu are with the Department of Photonics and the Institute of Electro-Optical Engineering, National Chiao Tung University, Hsinchu 30010, Taiwan (e-mail: potsung@mail.nctu.edu.tw; ricky.eo94g@nctu.edu.tw).

L.-H. Chiu was with the National Chiao Tung University, Hsinchu 30010, Taiwan. He is now with Taiwan Semiconductor Manufacturing Company Ltd., Hsinchu 30077, Taiwan (e-mail: leonard0129.di98g@g2.nctu.edu.tw).

Color versions of one or more of the figures in this paper are available online at http://ieeexplore.ieee.org.

Digital Object Identifier 10.1109/JLT.2012.2229695

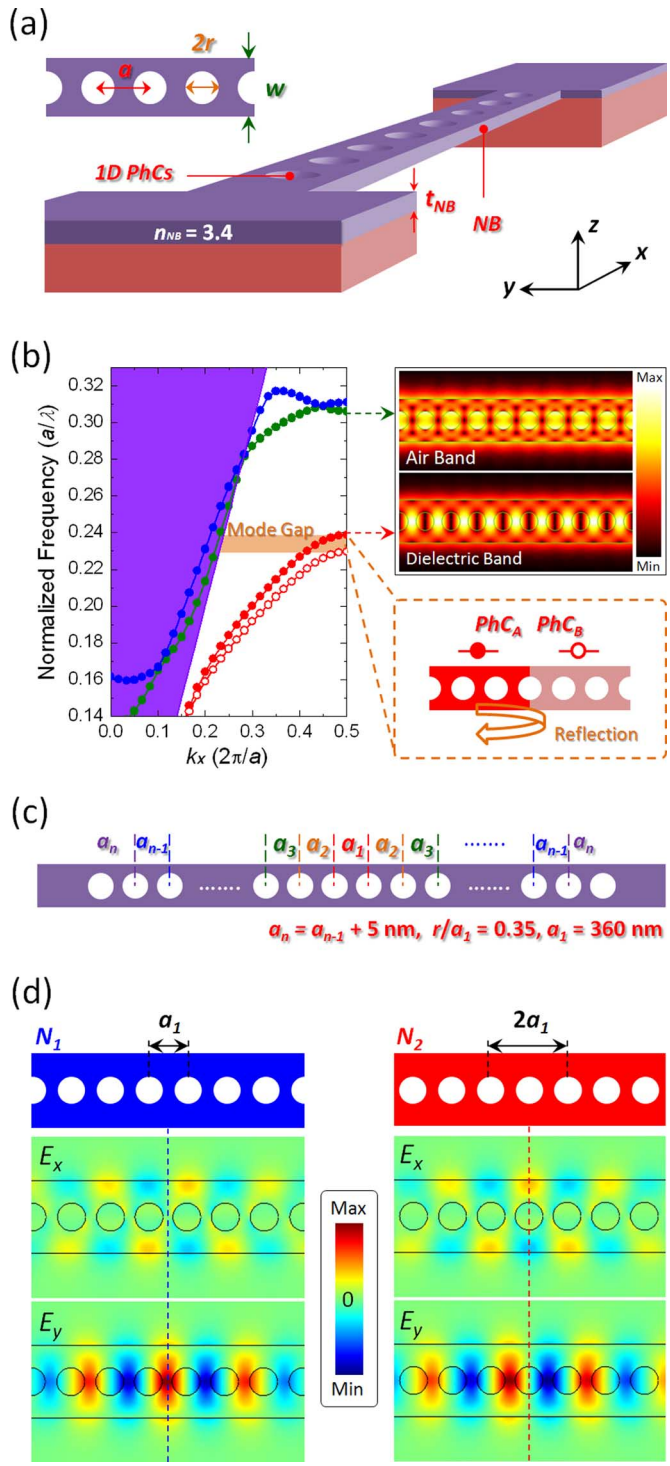

Fig. 1. (a) Scheme of a suspended *NB* with 1-D PhCs and (b) its TE-like propagating band diagram via 3-D PWE method. Theoretic $|E|^2$ field distributions of the dielectric and air bands in PWE simulations are shown as the inset of (b). Illustration of forming mode gap for the dielectric band by 1-D PhCs with different r/a on NB is also shown in (b). (c) Design of 1-D PhC NB nanocavity with mode gap confined dielectric band via lattice gradually shifted PhC mirrors. (d) Confined dielectric mode profiles in E_x and E_y fields in nanocavities with cavity sizes of a_1 (N_1) and $2a_1$ (N_2) obtained via 3-D FEM.

and PhC_B with different r/a can serve as a mirror and double heterointerfaces can form a nanocavity.

To precisely control different r/a of PhCs in fabrication, tuning lattice constant a is a more feasible way than tuning the air-hole radius r. Therefore, the PhC mirror of our nanocavity design shown in Fig. 1(c) is formed by n air holes with gradually increased lattice constant on both sides. From the center of the NB, under a fixed r of 126 nm, the lattice constant a_n is linearly increased by a 5 nm increment, where a_1 is 360 nm. Based on this design, we investigate the nanocavities with two different cavity sizes of a_1 and $2a_1$, named N_1 and N_2 nanocavities, as shown in Fig. 1(d), where the dielectric vein and air hole locate at the center of these two nanocavities, respectively.

To explore the dielectric modes in different nanocavities, the 3-D finite-element method (FEM) is utilized. The mode profiles in E_x and E_y fields of the zeroth-order dielectric modes confined in N_1 and N_2 nanocavities are shown in Fig. 1(d), where E_y is the dominant field component. Owing to different cavity geometries, the E_y fields in N_1 and N_2 nanocavities show even and odd symmetries, which lead to different dielectric mode properties. Via 3-D FEM, theoretic Q factors and mode volumes (V) of the zeroth-order dielectric modes in N_1 and N_2 nanocavities under different n from 4 to 18 are shown in Fig. 2(a). The Q factors of the dielectric modes in N_1 (Q_{N1}) and N_2 (Q_{N2}) nanocavities both increase with n and become saturated when $n > 14$, while Q_{N2} is always higher than Q_{N1} under different n. The difference in Q can be explained by the theoretic time-averaged power flows of the zeroth-order dielectric modes in N_1 and N_2 nanocavities at *xz* plane in Fig. 2(b) via 3-D FEM. In Fig. 2(b), less power flow above and below the slab means less optical loss of the zeroth-order dielectric mode in N_2 nanocavity, which is engineered by different E_y symmetries shown in Fig. 1(d) and makes Q_{N2} larger than Q_{N1}. When n is larger than 14, Q_{N1} and Q_{N2} reach as high as 1×10^6 and 3×10^6, respectively. In addition, the mode volume V of the zeroth-order dielectric mode in N_2 (V_{N2}) nanocavity is always slightly larger than that in N_1 (V_{N1}) nanocavity under different n due to the larger cavity size of N_2 nanocavity. When n is larger than 7, V_{N1} and V_{N2} are 0.37 $(\lambda/n)^3$ and 0.39 $(\lambda/n)^3$, respectively.

III. Dielectric Mode Lasing Properties From Nanocavities With Different Sizes

The designed N_1 and N_2 nanocavities are realized on the epitaxial structure consisted of compressively strained InGaAsP multi-quantum-wells (MQWs) with thickness of 220 nm grown on InP substrate via a series of electron-beam lithography with proximity correction, dry-, and wet-etching processes. The details can be found in our previous report [13]. Fig. 3 shows the tilted and top views of $1-$D PhC NB N_1 and N_2 nanocavities under scanning electron microscope (SEM), where $a_1, r/a_1, w$, and n are 360 nm, 0.37, 670 nm, and 8, respectively.

The N_1 and N_2 nanocavities are then optically pumped by a laser diode with wavelength of 845 nm, 15 ns pulse duration, and 100 kHz repetition rate at room temperature. The single-mode lasing spectra near 1550 nm and the light-in light-out (*L-L*) curves of $1-$D PhC NB N_1 and N_2 nanocavities are shown in Fig. 4(a) and (b). Via matching the mode frequencies with the simulation results, the lasing modes are addressed as the zeroth-order dielectric modes. Low threshold of 350 μW is obtained from the N_2 nanocavity. When considering the power

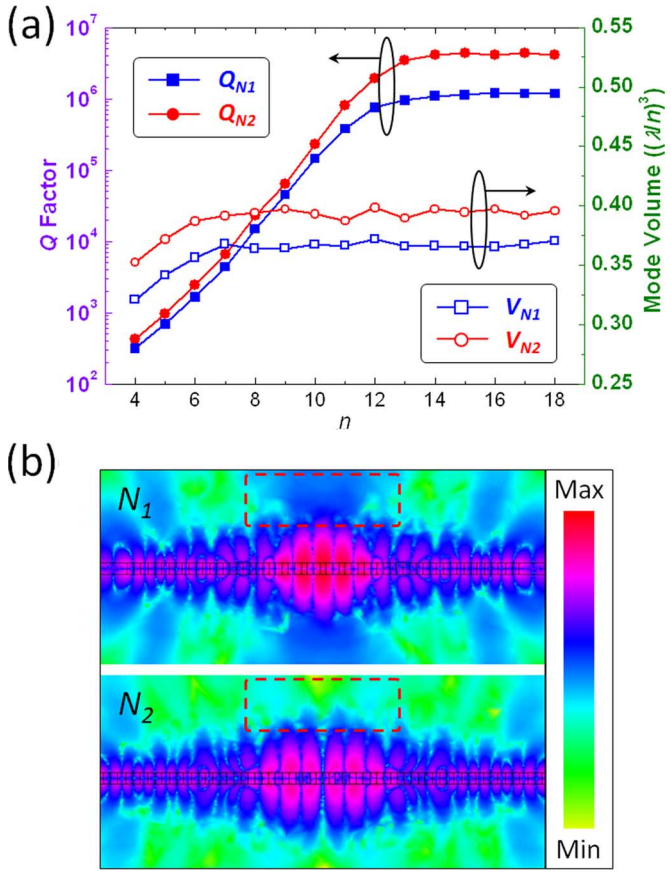

Fig. 2. (a) Theoretic Q and V of the zeroth-order dielectric modes in $1-$D PhC NB N_1 and N_2 nanocavities with varied n from 4 to 18 via 3-D FEM. (b) Time-averaged power flow distributions of the zeroth-order dielectric modes in $1-$D PhC NB N_1 and N_2 nanocavities with $n = 10$ at xz plane via 3-D FEM.

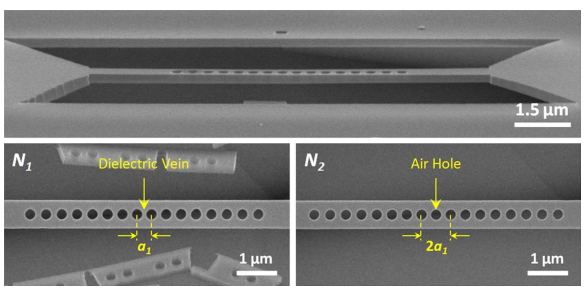

Fig. 3. Tilted- and top-view SEM pictures of 1D PhC NB N_1 and N_2 nanocavities.

absorbed by the MQWs, the effective threshold is only about 11 μW. Furthermore, we observe two reasonable phenomena from the L-L curves of N_1 and N_2 nanocavities with the same lattice parameters. First, the threshold of N_2 nanocavity ($\sim$350 μW) is smaller than that of N_1 nanocavity ($\sim$460 μW), which is always observed in all samples. This is because Q_{N2} is always higher than Q_{N1} under the same lattice parameters. Second, the slope efficiencies of the zeroth-order dielectric modes in N_1 nanocavities are always larger than those in N_2 nanocavities. This is because more energy radiates into the air by the zeroth-order dielectric mode in N_1 nanocavity than in N_2 nanocavity. This can be confirmed by their theoretic radiation patterns in $|E^2|$ fields (20 μm above the slabs) of the zeroth-order dielectric modes in these two nanocavities shown in Fig. 4(c), where the dielectric mode in N_1 nanocavity shows stronger vertically directional emission than that in N_2 nanocavity. These two phenomena show that the modal symmetries can greatly affect the lasing properties, including the lasing thresholds and emission directions/intensities. Moreover, the lasing emissions from the N_1 and N_2 nanocavities are both linearly polarized, as shown in the inset of Fig. 4(b). This is the nature of the dielectric modes dominated by the E_y fields, as predicted in Fig. 1(d).

With large PhC mirror periods, for example, $n = 18$ shown in Fig. 5(a), the first-order dielectric mode is observed in the lasing spectra shown in Fig. 5(b), which is addressed by matching the measured frequencies with the simulation results. In addition, we also change the positions of pump spot ($\sim$1.5 μm in diameter) from the cavity center to the outer PhC mirror, as indicated in Fig. 5(a) via a Piezo stage with 30 nm step resolution, to verify the difference in mode localizations between the zeroth- and first-order dielectric modes. The lasing spectra under different pump position shifts s from 0 (cavity center) to 1.35 μm are shown in Fig. 5(b). When s increases, the first-order dielectric mode starts to dominate the lasing properties under a fixed pump power of 1.4 mW. When s becomes larger than 1.20 μm, only the first-order dielectric mode is excited. This pump position dependence is obviously caused by the different field localizations of the zeroth- and first-order dielectric modes shown in Fig. 5(c).

IV. High-Order Modes in *NB* Nanocavities With Large PhC Mirror Periods

One can increase the Q value by adding more PhC mirror periods [22], [23] in various 1-D PhC NB nanocavities, as we predicted in Fig. 2(a). However, high-order modes will appear as we observed in Fig. 5(b), which is not preferred for a nanolaser source. In experiments, we investigate the high-order modes in N_1 nanocavity with different n of 8, 10, and 14. The spectra shown in Fig. 5(d) are obtained under a fixed pump power of 1.5 mW. With $n = 8$, the nanocavity shows the zeroth-order dielectric mode single-mode lasing. When n increases to be 10 and 14, the first- and second-order dielectric modes appear in sequence. This is because adding more PhC mirror periods increases the Q factors of the zeroth-order and the high-order dielectric modes simultaneously [24]. This makes the high-order modes become competitive in lasing. When n of the N_1 nanocavity increases from 8 to 14, the Q factors of the first- and second-order dielectric modes increase from 500 and 148 to be 4.1×10^4 and 2×10^3, respectively. Furthermore, the increased Q factors of high-order modes also significantly increase the threshold of the zeroth-order dielectric mode lasing, which is not beneficial for a nanolaser source. Thus, for active nanolaser applications, large PhC mirror periods may not be the essentials. The nanocavity should be with PhC mirror periods sufficient for only the zeroth-order dielectric mode lasing, while the device footprint can be kept very small (for $n = 8$, device footprint $\sim$15 μm^2 only, which is smaller than that we reported previously [13]). The device footprint is defined as the maximum area where the coupling effect cannot be neglected when other devices exist nearby. Therefore, in addition to the area of PhC

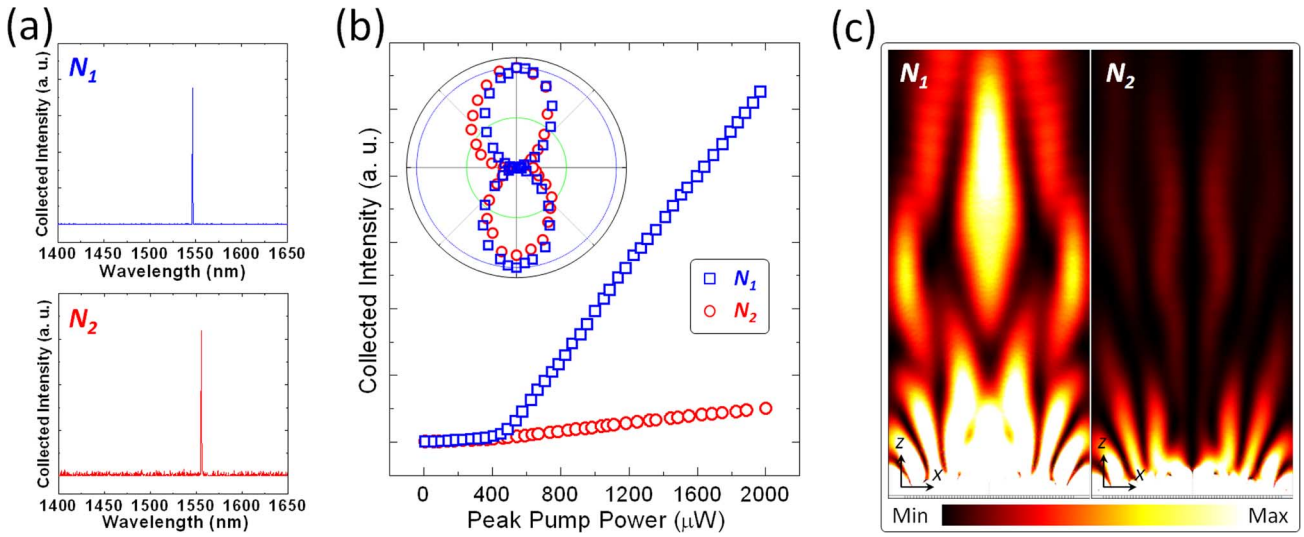

Fig. 4. (a) Single-mode lasing spectra, (b) L-L curves, and measured linear polarizations of the zeroth-order dielectric modes in $1-$ D PhC NB N_1 and N_2 nanocavities with the same lattice parameters. (c) Theoretic radiation patterns of the dielectric modes in $1-$ D PhC NB N_1 and N_2 nanocavities with $n = 8$ at xz plane.

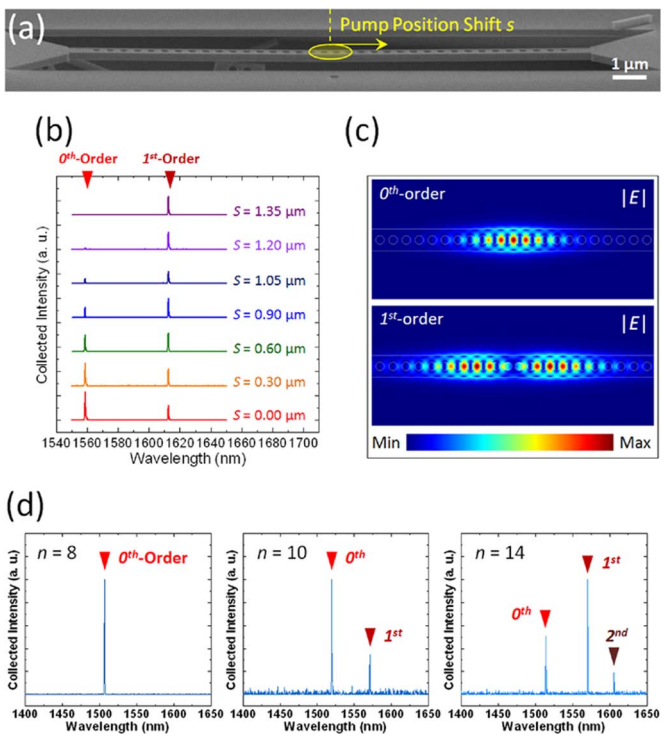

Fig. 5. (a) SEM picture and (b) lasing spectra when moving the pump position away from the center of $1-$ D PhC NB N_1 nanocavity with $n = 18$ via a Piezo stage. The first-order dielectric mode dominates the lasing when the pump position shift s is more than 1.20 μm away from the nanocavity center. (c) Zeroth- and first-order dielectric mode profiles in electric fields in $1-$ D PhC NB N_1 nanocavity with $n = 10$ obtained via 3-D FEM. (d) Lasing spectra of $1-$ D PhC NB N_1 nanocavities with $n = 8$, 10, and 14.

NB, the air regions with half-wavelength thickness on each side of the NB are also included in the calculation of device footprint, which is different from the definition in our previous report [13].

V. Coupled Dielectric Modes in Width-Mismatched Coupled NB Nanocavity

In addition to the nanocavity on single NB, one can also put two identical NB nanocavities side by side to form a coupled NB nanocavities [17], [20], [25]–[27] for various applications, for example, optomechanical nano-resonators [17], optical sensors [20], tunable lasers [26], optical filters [27], and so on. Bonding and antibonding modes analog to the energy states in a two-atom system can be obtained in this coupled structure to form a photonic molecule. In experiments, we demonstrate a coupled *NB* laser based on $1-$ D PhC N_2 nanocavities, as shown in Fig. 6(a). The 150 nm air gap distance g between the two NBs is shorter than the mode field decay length into the air and sufficient for producing strong coupling between the nanocavities. Two peaks are observed from the device as shown in Fig. 6(b) and addressed as the bonding and antibonding modes via 3-D FEM simulations. Theoretic antibonding mode profile in E_y field in Fig. 6(c) will show higher field confinement factor in dielectric (~ 0.425) than that of bonding mode (~ 0.405).

In the literature, researchers always assume that the two *NB* nanocavities are identical. However, different detunes between the *NBs* can be easily produced by various fabrication imperfections. For example, if there exists 15 nm beamwidth mismatch M (upper $w = 655$ nm, lower $w = 670$ nm, M is defined as [lower w-upper w)] between 1-D PhC coupled NB N_2 nanocavities with $g = 250$ nm, $n = 10$, and r/a_1 of 0.365, the E_y fields of bonding and antibonding modes will tend to concentrate in different NBs, as shown in Fig. 7(a). This is because the coupling strength is greatly affected by the frequency difference of the dielectric modes in upper and lower NBs. When the NBs are identical, the same dielectric mode frequencies in the NBs lead to strong coupling. However, once a detune between the NBs is induced, for example, the NB width mismatch here, the dielectric mode frequencies in upper and lower NBs are different, and the coupling between them becomes weak. Owing to the weak coupling, each coupled dielectric mode will

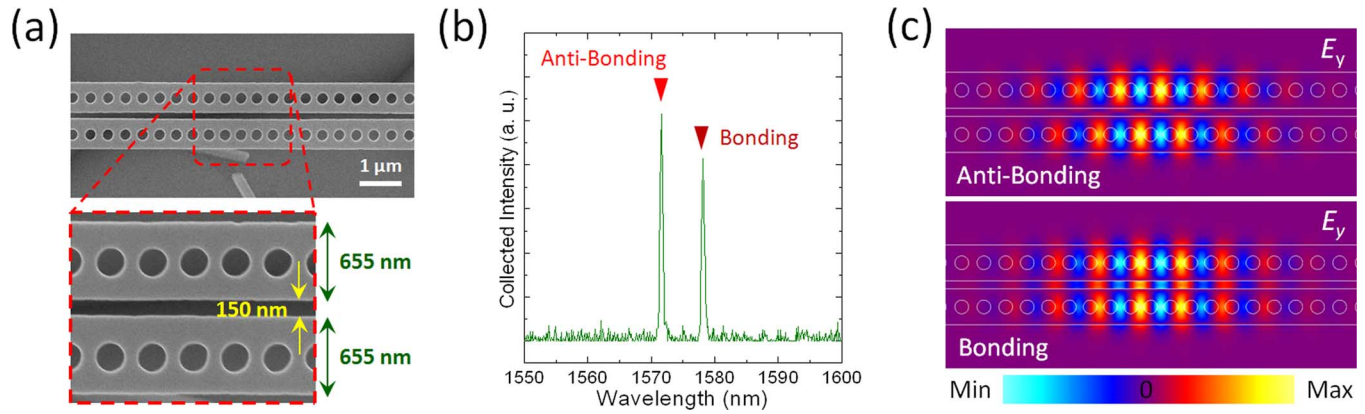

Fig. 6. (a) Top-view SEM pictures of 1-D PhC coupled NB N_2 nanocavities with $w = 655$ nm, $g = 150$ nm, $n = 10$, and $r/a_1 = 0.345$. (b) Two peaks in spectrum correspond to the bonding and antibonding modes. (c) The ideal bonding and antibonding mode profiles in E_y fields in 1-D PhC coupled NB N_2 nanocavities.

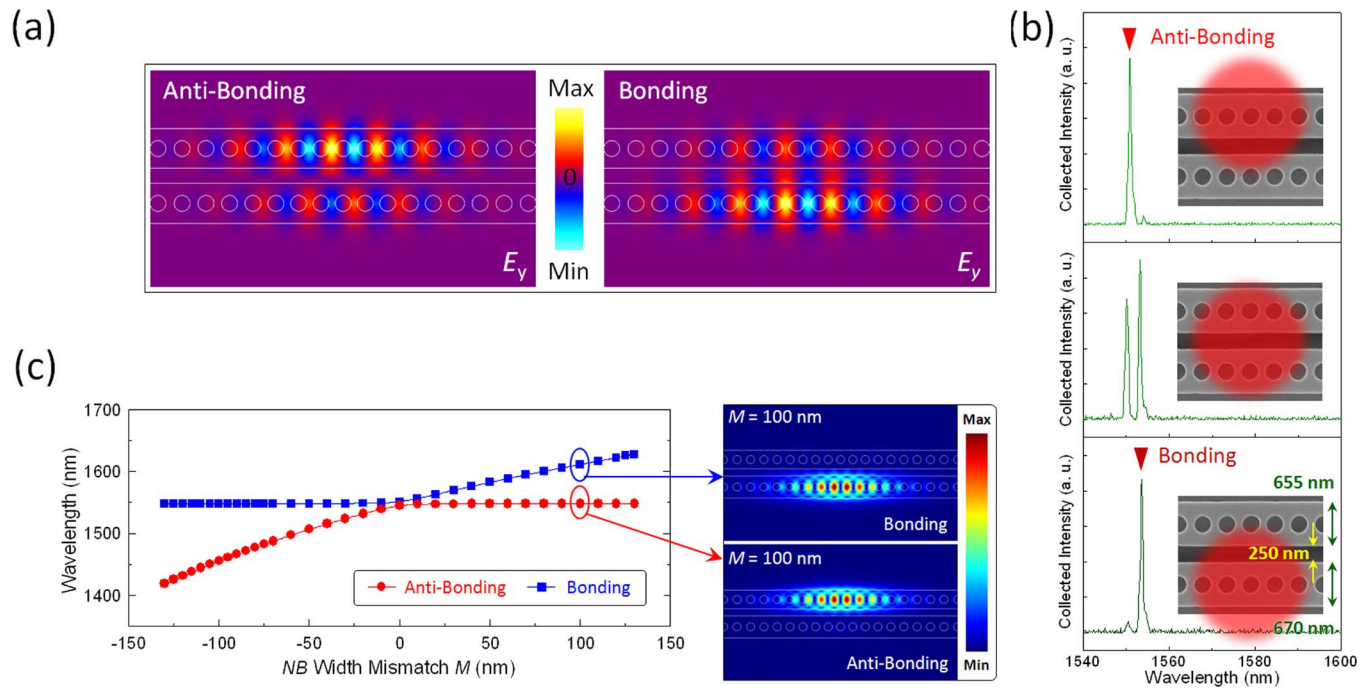

Fig. 7. (a) Theoretic bonding and antibonding mode profiles in E_y fields in 1-D PhC coupled NB N_2 nanocavities with $M = 15$ nm (upper $w = 655$ nm, lower $w = 670$ nm), $g = 250$ nm, $n = 10$, and r/a_1 of 0.365. (b) Spectra of dominant lasing mode switching between the bonding and antibonding modes via spatially nonuniform optical pumping in 1-D PhC coupled NB N_2 nanocavities with the same parameters in (a). (c) Theoretic wavelengths of the bonding and antibonding modes in 1-D PhC coupled NB N_2 nanocavity with gap size of 200 nm under different M. Theoretic mode profiles in electric fields of bonding and antibonding modes under $M = 100$ nm are also shown as the insets.

more concentrate in either NB. For the dielectric mode in the narrower NB with shorter wavelength, the coupling mode will be in the form of antibonding state with higher energy. Likewise, the coupling of dielectric mode with longer wavelength in the wider NB will be the bonding state.

In experiments, from the coupled NB N_2 nanocavities with M of 15 nm and lattice parameters in above simulation, the dominant lasing mode will switch from the antibonding to the bonding modes when the pump position is moved from the upper to the lower NB, as shown in Fig. 7(b). This phenomenon agrees with the bonding and antibonding mode profiles in E_y fields shown in Fig. 7(a) and implies that one can control which coupled mode is the dominant lasing mode via selectively injecting carriers into one of the NBs.

In addition, we further enlarge the beamwidth mismatch M in a 1-D PhC coupled NB with gap size of 200 nm in simulation. Theoretic wavelengths of bonding and antibonding modes shown in Fig. 7(c) under different M can be analog to the coupled energy states variations in a two-atom system with asymmetric atom sizes. When M is large, the bonding and antibonding modes become more isolated than the cases with small M, which can be clearly observed form the mode profiles of the bonding and antibonding modes under $M = 100$ nm shown as the insets of Fig. 7(c). With large beamwidth mismatch, large coupled mode wavelength differences can also be obtained on-demand in this 1-D PhC coupled NB for various applications in PICs. The extended results and discussions of this issue will be published elsewhere [28].

VI. Conclusion

In this study, we study 1-D PhC NB nanocavities with mode gap confined dielectric modes, where the PhC mirror with mode gap is formed via gradually increasing the lattice constant. We investigate and compare the zeroth-order dielectric modal properties in N_1 and N_2 nanocavities with different cavity sizes. In simulations, high Q of 3×10^6 and small mode volume of $0.39(\lambda/n)^3$ are obtained from the zeroth-order dielectric mode in N_2 nanocavity. In experiments, the zeroth-order dielectric modes lasing with low effective thresholds are obtained from N_1 and N_2 nanocavities. Both in simulations and experiments, we have shown that the different dielectric modal symmetries in these two nanocavities with different geometries lead to very different lasing properties, including *Qs*, thresholds, and emission directions/intensities. In addition, to avoid the rising of high-order modes, we point out that the presented design for serving as a nanolaser should be with PhC mirror periods sufficient for only the zeroth-order dielectric mode lasing, while the device footprint can be kept very small (for $n = 8$, device footprint $\sim 15\ \mu\text{m}^2$). Furthermore, we also show that the bonding and antibonding modes in 1-D PhC coupled NB N_2 nanocavities will exhibit nonuniform mode distributions owing to the beamwidth mismatch between NBs. Via their mode fields concentrated in either NBs, we can decide and control the dominant lasing mode via spatially nonuniform carrier injection, which would be beneficial for switchable nanolasers. Finally, we also theoretically show that large coupled mode wavelength differences can be obtained on-demand in 1-D PhC coupled NB via tuning the beamwidth mismatch on purpose for various applications in PICs.

Acknowledgment

The authors would like to thank the help from Center for Nano Science & Technology, National Chiao Tung University, Taiwan.

References

[1] B. S. Song, S. Noda, T. Asano, and Y. Akahane, "Ultra-high-Q photonic double-heterostructure nanocavity," *Nat. Mater.*, vol. 4, pp. 207–210, 2005.

[2] Y. Akahane, T. Asano, B. S. Song, and S. Noda, "High-Q photonic nanocavity in a two-dimensional photonic crystal," *Nature*, vol. 425, pp. 944–947, 2003.

[3] H. G. Park, S. H. Kim, S. H. Kwon, Y. G. Ju, J. K. Yang, J. H. Baek, S. B. Kim, and Y. H. Lee, "Electrically driven single-cell photonic crystal laser," *Science*, vol. 305, pp. 1444–1447, 2004.

[4] S. Kita, K. Nozaki, and T. Baba, "Refractive index sensing utilizing a cw photonic crystal nanolaser and its array configuration," *Opt. Exp.*, vol. 16, pp. 8174–8180, 2008.

[5] S. Matsuo, A. Shinya, T. Kakitsuka, K. Nozaki, T. Segawa, T. Sato, Y. Kawaguchi, and M. Notomi, "High-speed ultracompact buried heterostructure photonic-crystal laser with 13 fJ of energy consumed per bit transmitted," *Nat. Photon.*, vol. 4, pp. 648–654, 2010.

[6] K. J. Vahala, "Optical microcavities," *Nature*, vol. 424, pp. 839–846, 2003.

[7] J. S. Foresi, P. R. Villeneuve, J. Ferrera, E. R. Thoen, G. Steinmeyer, S. Fan, J. D. Joannopoulos, L. C. Kimerling, H. I. Smith, and E. P. Ippen, "Photonic-bandgap microcavities in optical waveguide," *Nature*, vol. 390, pp. 143–145, 1997.

[8] M. Notomi, E. Kuramochi, and H. Taniyama, "Ultrahigh-Q nanocavity with 1D photonic gap," *Opt. Exp.*, vol. 16, pp. 11095–11102, 2008.

[9] P. B. Deotare, M. W. McCutcheon, I. W. Frank, M. Khan, and M. Lončar, "High quality factor photonic crystal nanobeam cavities," *Appl. Phys. Lett.*, vol. 94, pp. 121106-1–121106-3, 2009.

[10] Y. Zhang and M. Lončar, "Ultra-high quality factor optical resonators based on semiconductor nanowires," *Opt. Exp.*, vol. 16, pp. 17400–17409, 2008.

[11] Y. Gong, B. Ellis, G. Shambat, T. Sarmiento, J. S. Harris, and J. Vučković, "Nanobeam photonic crystal cavity quantum dot laser," *Opt. Exp.*, vol. 18, pp. 8781–8789, 2010.

[12] Y. Zhang, M. Khan, Y. Huang, J. H. Ryou, P. B. Deotare, R. Dupuis, and M. Lončar, "Photonic crystal nanobeam lasers," *Appl. Phys. Lett.*, vol. 97, pp. 051104-1–051104-3, 2010.

[13] T. W. Lu, L. H. Chiu, P. T. Lin, and P. T. Lee, "One-dimensional photonic crystal nanobeam lasers on a flexible substrate," *Appl. Phys. Lett.*, vol. 99, pp. 071101-1–071101-3, 2011.

[14] Q. Quan, P. B. Deotare, and M. Lončar, "Photonic crystal nanobeam cavity strongly coupled to the feeding waveguide," *Appl. Phys. Lett.*, vol. 96, pp. 203102-1–203102-3, 2010.

[15] X. Chew, G. Zhou, F. S. Chau, J. Deng, X. Tang, and Y. C. Loke, "Dynamic tuning of an optical resonator through MEMS-driven coupled photonic crystal nanocavities," *Opt. Lett.*, vol. 35, pp. 2517–2519, 2010.

[16] L. D. Haret, T. Tanabe, E. Kuramochi, and M. Notomi, "Extremely low power optical bistability in silicon demonstrated using 1D photonic crystal nanocavity," *Opt. Exp.*, vol. 17, pp. 21108–21117, 2009.

[17] M. Eichenfield, J. Chan, R. Camacho, K. J. Vahala, and O. Painter, "Optomechanical crystals," *Nature*, vol. 462, pp. 78–82, 2009.

[18] S. Mandal, X. Serey, and D. Erickson, "Nanomanipulation using silicon photonic crystal resonators," *Nano Lett.*, vol. 10, pp. 99–104, 2009.

[19] S. Mandal and D. Erickson, "Nanoscale optofluidic sensor arrays," *Opt. Exp.*, vol. 16, pp. 1623–1631, 2008.

[20] B. Wang, M. A. Dündar, R. Nötzel, F. Karouta, S. He, and R. W. van der Heijden, "Photonic crystal slot nanobeam slow light waveguides for refractive index sensing," *Appl. Phys. Lett.*, vol. 97, pp. 151105-1–151105-3, 2010.

[21] A. R. M. Zain, N. P. Johnson, M. Sorel, and R. M. De La Rue, "Ultra high quality factor one dimensional photonic crystal/photonic wire micro-cavities in silicon-on-insulator (SOI)," *Opt. Exp.*, vol. 16, pp. 12084–12088, 2008.

[22] M. W. McCutcheon and M. Lončar, "Design of a silicon nitride photonic crystal nanocavity with a quality factor of one million for coupling to a diamond nanocrystal," *Opt. Exp.*, vol. 16, pp. 19136–19145, 2008.

[23] J. Chan, M. Eichenfield, R. Camacho, and O. Painter, "Optical and mechanical design of a "zipper" photonic crystal optomechanical cavity," *Opt. Exp.*, vol. 17, pp. 3802–3817, 2009.

[24] Y. Takahashi, Y. Tanaka, H. Hagino, T. Asano, and S. Noda, "Higher-order resonant modes in a photonic heterostructure nanocavity," *Appl. Phys. Lett.*, vol. 92, pp. 241910-1–241910-3, 2008.

[25] P. B. Deotare, M. W. McCutcheon, I. W. Frank, M. Khan, and M. Lončar, "Coupled photonic crystal nanobeam cavities," *Appl. Phys. Lett.*, vol. 95, pp. 031102-1–031102-3, 2009.

[26] R. Perahia, J. D. Cohen, S. Meenehan, T. P. M. Alegre, and O. Painter, "Electrostatically tunable optomechanical "zipper" cavity laser," *Appl. Phys. Lett.*, vol. 97, pp. 191112-1–191112-3, 2010.

[27] X. Chew, G. Zhou, F. S. Chau, and J. Deng, "Nanomechanically tunable photonic crystal resonators utilizing triple-beam coupled nanocavities," *IEEE Photon. Technol. Lett.*, vol. 23, no. 18, pp. 1310–1312, Sep. 2011.

[28] T. W. Lu and P. T. Lee, "Couple modes in mismatched photonic crystal coupled nanobeams," in to be submitted.

Po-Tsung Lee (M'06) received the B.S. degree from the Department of Physics, National Taiwan University, Taipei, Taiwan, in 1997, and the M.S. and Ph.D. degrees from the Department of Electrical Engineering-Electrophysics, University of Southern California, Los Angeles, in 1998 and 2003, respectively.

During the Ph.D. study, she was involved in photonic crystal microcavity lasers. In 2003, she joined the Institute of Electro-Optical Engineering, National Chiao Tung University (NCTU), Hsinchu, Taiwan, as an Assistant Professor, where in 2007, she became an Associate Professor in the Department of Photonics. Her recent research interests are III–V semiconductor photonic crystal active and passive devices and their applications, metallic nanostructures with localized surface plasmon resonances, and silicon-based solar cell technologies.

Dr. Lee was the recipient of the University of Southern California Women in Science and Engineering Award in 2000–2001. She received the "Excellent Young Electrical Engineer Award" of the Chinese Institute of Electrical Engineering in 2011.

Tsan-Wen Lu received the B.S. degree from the Department of Electrical Engineering, National Tsing Hua University, Hsinchu, Taiwan, in 2003. He then received the M.S. and Ph.D. degrees from the Institute of Electro-Optical Engineering, National Chiao Tung University (NCTU), Hsinchu, in 2005 and 2009, respectively.

He is currently a Postdoctoral Fellow at NCTU. His recent research interests include photonic-crystal-based light emitters and localized surface plasmon resonance in metallic nanostructures.

Li-Hsun Chiu received the B.S. degree from the Department of Biomedical Engineering and Environmental Sciences, National Tsing Hua University, Hsinchu, Taiwan, in 2009, and the M.S. degree from the Display Institute, National Chiao Tung University (NCTU), Hsinchu, in 2011.

His research was focused on 1-D photonic crystal nanobeam light emitters. He is currently a R&D Engineer in Taiwan Semiconductor Manufacturing Company, Hsinchu.